6ICEGE 6th International Conference on Earthquake Geotechnical Engineering
1-4 November 2015
Christchurch, New Zealand

# Evaluation of Ground Deformations during the 2010-2011 Canterbury Earthquake Sequence

D. Bouziou[1], T. D. O'Rourke[2], M. Cubrinovski[3] and D. Henderson[4]

## ABSTRACT

A statistical analysis of liquefaction-induced ground deformations, expressed as differential vertical ground movement and lateral ground strain, during the 2010-2011 Canterbury Earthquake Sequence in New Zealand is presented. Liquefaction-induced ground deformations are calculated from high resolution light detection and ranging (LiDAR) data collected before and after each of the 4 Sept. 2010, 22 Feb. 2011, and 13 June 2011 earthquakes, and are evaluated in a special study area of reduced LiDAR error. The data are well described by the generalized extreme value distribution and indicate that the most severe local ground deformations are associated with the 4 Sept. 2011 earthquake, whereas the most widespread deformations occurred during the 22 Feb. 2011 earthquake. The highest values of differential vertical ground movement show a remarkably high degree of spatial correlation with natural waterways. Lateral strains along concrete perimeter footings and differential vertical ground floor displacements obtained from residential building surveys are in broad agreement with lateral strains and differential settlements derived from LiDAR measurements.

## Introduction

High resolution airborne light detection and ranging (LiDAR) data for vertical and lateral ground surface movements were collected before and after each main event of the Canterbury Earthquake Sequence (CES), and are used for the statistical evaluation of liquefaction-induced ground deformations. LiDAR-based liquefaction-induced ground deformation is expressed as lateral ground strain and ground angular distortion. Statistical distributions of these liquefaction-induced ground deformations and best fit probability distributions are presented. The relationship between LIDAR-based ground and residential building deformation is investigated from survey data for buildings damaged by liquefaction-induced ground movements.

## LiDAR Data

Airborne Light Detection and Ranging (LiDAR) surveys were flown at Christchurch. The data from airborne LiDAR surveys before and after each main Canterbury Earthquake Sequence (CES) earthquake were used by GNS Science under contract with Tonkin & Taylor Pty Ltd (T&T) to determine horizontal and vertical ground movements. Differential vertical ground

[1]Civil Engineer, Edafos Engineering Consultants S.A., Iperidou 9, Athens 10558, Greece, db552@cornell.edu
[2]Thomas R. Briggs Professor, 273 Hollister Hall, Cornell University, Ithaca, NY 14853, tdo1@cornell.edu
[3]Professor, Department of Civil and Natural Resources Engineering, Private Bag 4800, University of Canterbury, Christchurch, New Zealand 8140, misko.cubrinovski@canterbury.ac.nz
[4]Site Engineer, Downer New Zealand, 130 Kerrs Road, Wiri, Auckland, New Zealand 2104, Duncan.Henderson@downer.co.nz

movements were calculated from bare earth digital elevation models (DEMs) at 5-m spacing. LiDAR lateral movements were assessed at 4-m and 8-m spacing, and also averaged to provide lateral movements at 56-m spacing. They were calculated using a sub-pixel correlation method developed by Imagin'Labs Corporation, Pasadena, CA, and California Institute of Technology (Beavan et al., 2012). The fundamental LiDAR vertical accuracy after the 4 September 2011 earthquake is between ± 7 cm and ± 15 cm, whereas the LiDAR horizontal accuracy, compared to land survey measurements, is 40 to 55 cm (CERA, 2012).

## Study Area

Within a special study area, locations of high density vegetation and multi-story building damage were removed from the LiDAR data to reduce measurement error. The study area is shown in Figure 1. Areas greater than 0.1 $km^2$ and covered by vegetation (areas No. 2 through No. 10) were identified in ArcMap 10.1 software by Esri, Redlands, CA, using geospatial data from LINZ (2013), and were removed from the study area. The Christchurch Central Business District (CBD), identified as area No.1, was also excluded due to errors related to building damage.

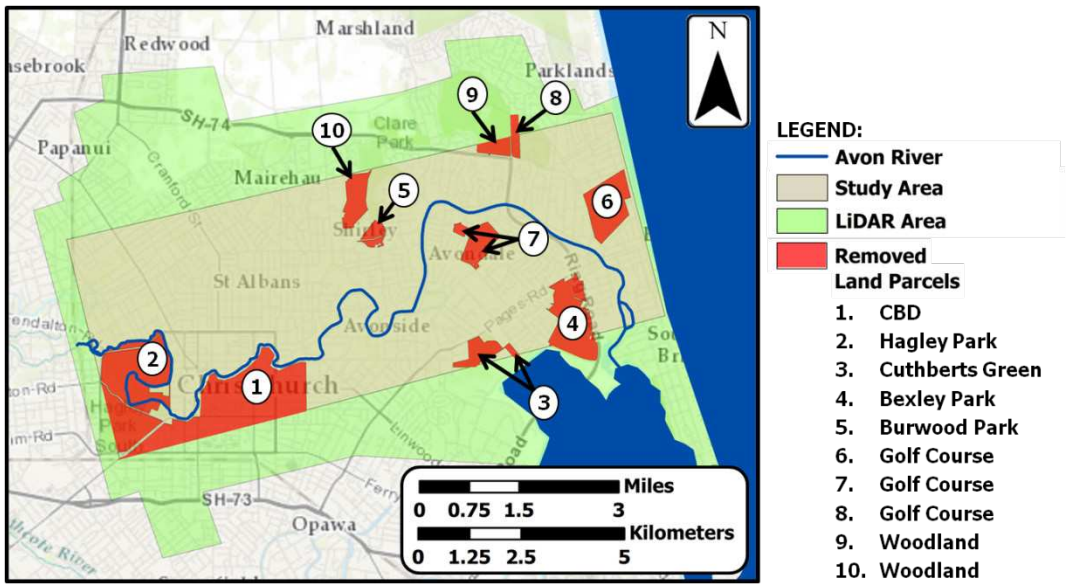


Figure 1: Study area and removed land parcels superimposed on the LiDAR area in Christchurch.

## Statistical Analysis of Differential Vertical Ground Movement and Lateral Ground Strain

Angular distortion, β, which is differential vertical movement divided by the horizontal distance between measurement points, was selected as the main vertical movement parameter. The horizontal deformation parameter was chosen as the absolute value of maximum ground strain, $\varepsilon_{HP}$. The vertical and horizontal ground surface movements developed by pairs of high-resolution LiDAR data sets were used to calculate β and $\varepsilon_{HP}$ at 5-m and 4-m spacing, respectively. The calculation of β and $\varepsilon_{HP}$ was performed for each main seismic event using the methods described by O'Rourke et al. (2014) and Bouziou (2015). Such parameters are used frequently to evaluate ground movement effects on buildings (e.g., Boscardin and Cording, 1989).

***The generalized extreme value distribution***

When analyzing the statistical distributions of ground movement for the CES main shocks, many different mathematical formulations were investigated, and it was found that the generalized extreme value distribution (GEV) provides the best fit for β and $\varepsilon_{HP}$, as follows:

$$f(x|\gamma_{GEV},\mu_{GEV},\sigma_{GEV}) = \frac{1}{\sigma_{GEV}} exp\left(-\left(1+\gamma_{GEV}\frac{(x-\mu_{GEV})}{\sigma_{GEV}}\right)^{-\frac{1}{\gamma_{GEV}}}\right)\left(1+\gamma_{GEV}\frac{(x-\mu_{GEV})}{\sigma_{GEV}}\right)^{-1-\frac{1}{\gamma_{GEV}}} \quad (1)$$

for $1+\gamma_{GEV}\frac{(x-\mu_{GEV})}{\sigma_{GEV}} > 0$ and $\gamma_{GEV} \neq 0$

in which $\mu_{GEV}$ is the location parameter that determines the location or shift of the distribution, $\sigma_{GEV}$ is the scale parameter that determines the statistical dispersion of the distribution, and $\gamma_{GEV}$ is the shape parameter that affects the shape of the distribution. The Matlab function gevfit was used to estimate these parameters and corresponding confidence intervals.

***Differential vertical ground movement***

Cumulative distributions of β for the 4 Sept. 2010, the 22 Feb. 2011, and the 13 June 2011 earthquakes are presented in Figure 2. Unrealistically high values of $\beta \geq 30x10^{-3}$, which represent 3% to 5% of the population, were screened from the data for additional error reduction. As shown in Figure 2, the GEV distribution provides a good fit for each event.

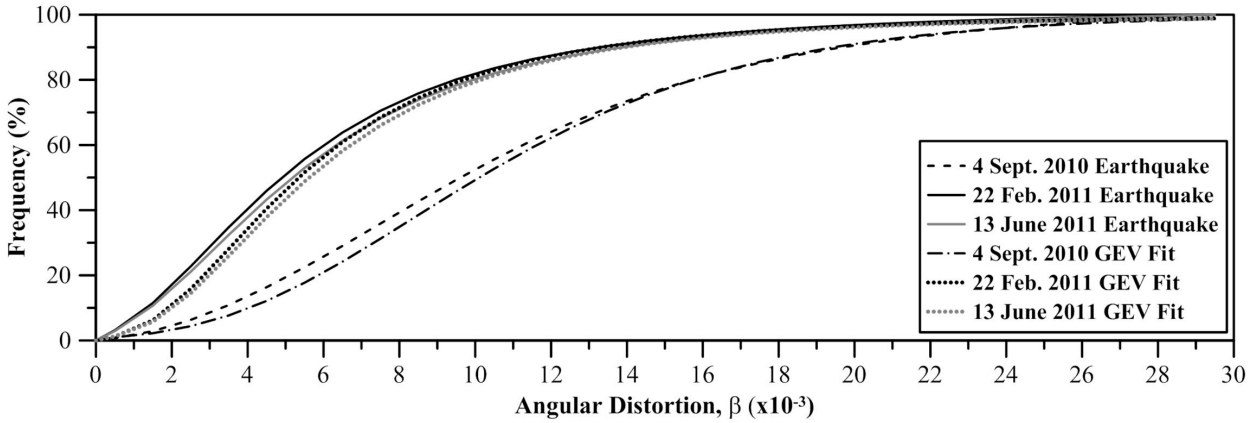


Figure 2: Cumulative distributions of LiDAR-based ground angular distortions in the study area during the 4 Sept. 2010, 22 Feb. 2011, and 13 June 2011 earthquakes.

There is a remarkable similarity in the cumulative distributions for the 22 Feb. 2011, and 13 June 2011 earthquakes, and a marked difference in same for the 4 Sept. 2010 earthquake. Although β for the 4 Sept. 2010 earthquake was locally more severe compared to the other earthquakes, liquefaction was less extensive in terms of spatial coverage of approximately 52 $km^2$, or 32% of the Christchurch area (Bouziou, 2015). In contrast, approximately 96 $km^2$ and 91 $km^2$ (66% and 62% of the Christchurch area, respectively) were associated with liquefaction during the 22 Feb. 2011 and 13 June 2011 earthquakes, respectively. Slumping and heave along the Avon River and

Horseshoe Lake may have diminished local slopes and elevation gradients so that liquefaction effects in subsequent earthquakes, although more extensive, were less severe overall with respect to angular distortion.

***Lateral ground strain***

Figure 3 shows the cumulative distributions of LiDAR-based tensile and compressive $\varepsilon_{HP}$ for the 4 Sept. 2010, 22 Feb. 2011, and 13 June 2011 earthquakes. Very high values of $\varepsilon_{HP} > 3\%$, which represent 3% to 5% of the population, were screened from the data to reduce errors. The GEV distributions for tensile and compressive $\varepsilon_{HP}$ are nearly the same for each earthquake, with the largest lateral strains corresponding to the 4 Sept. 2010 earthquake.

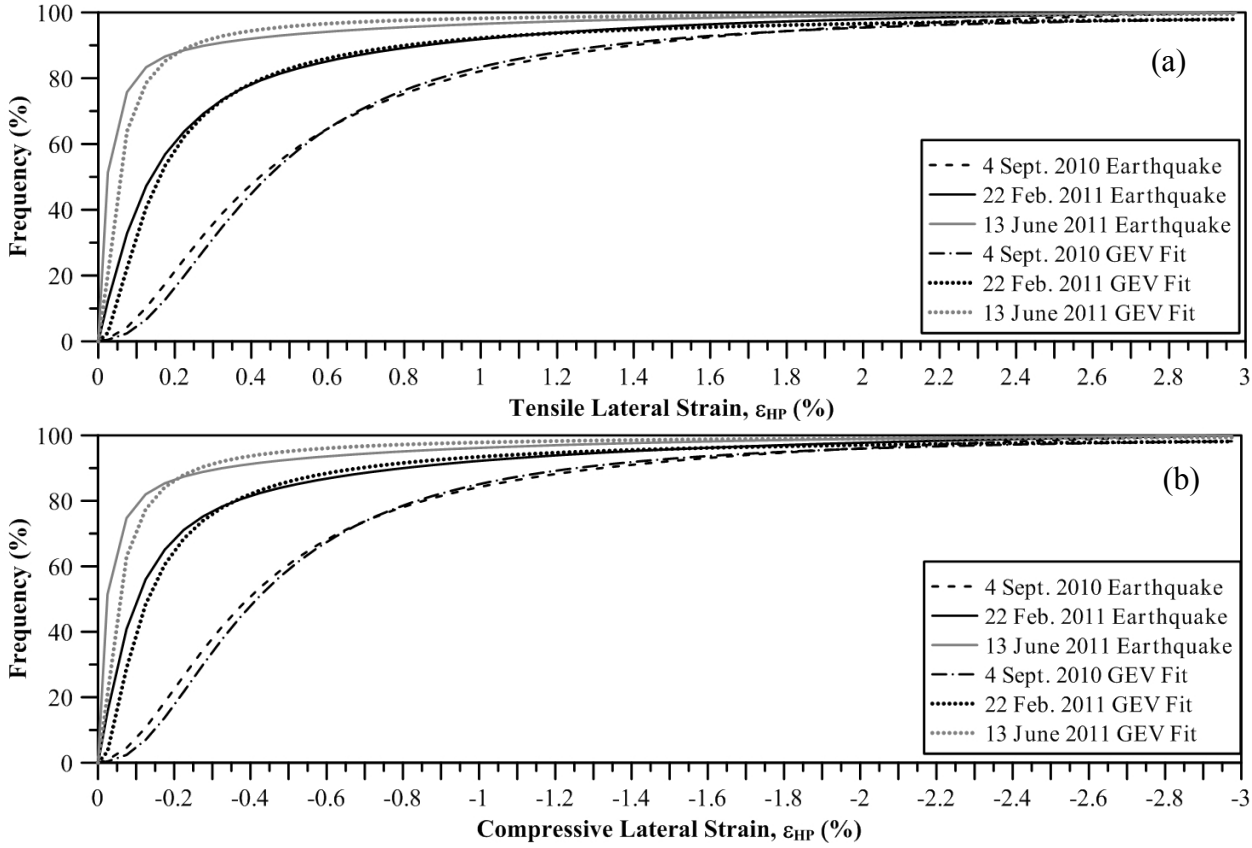


Figure 3: Cumulative distributions of LiDAR-based a) tensile, and b) compressive lateral ground strain in the study area during the 4 Sept. 2010, 22 Feb. 2011, and 13 June 2011 earthquakes.

***Statistical screening of ground deformation patterns***

Statistical distributions for $\beta$ and $\varepsilon_{HP}$ in the study area were used to locate the largest ground deformations. Values of $\beta$ and $\varepsilon_{HP}$, representing the upper 2.5% of the data in Figures 2 and 3, respectively, were located within the study area shown in Figure 1. Locations of $\beta > 21.3 \times 10^{-3}$, representing 2.5% of the population, are shown in Figure 4a. They align themselves with locations adjacent to the Avon River and its cut-off meanders, such as Horseshoe Lake and Porritt Park, and in areas of natural waterways. Similarly, the population of $\varepsilon_{HP} > 1.9\%$,

representing 2.5% of the population, are shown in Figure 4b. They are concentrated close to the Avon River, Horseshoe Lake, and areas affected by lateral spreading, such as Porritt Park, Anzac Drive, and Queen Elizabeth II Stadium.

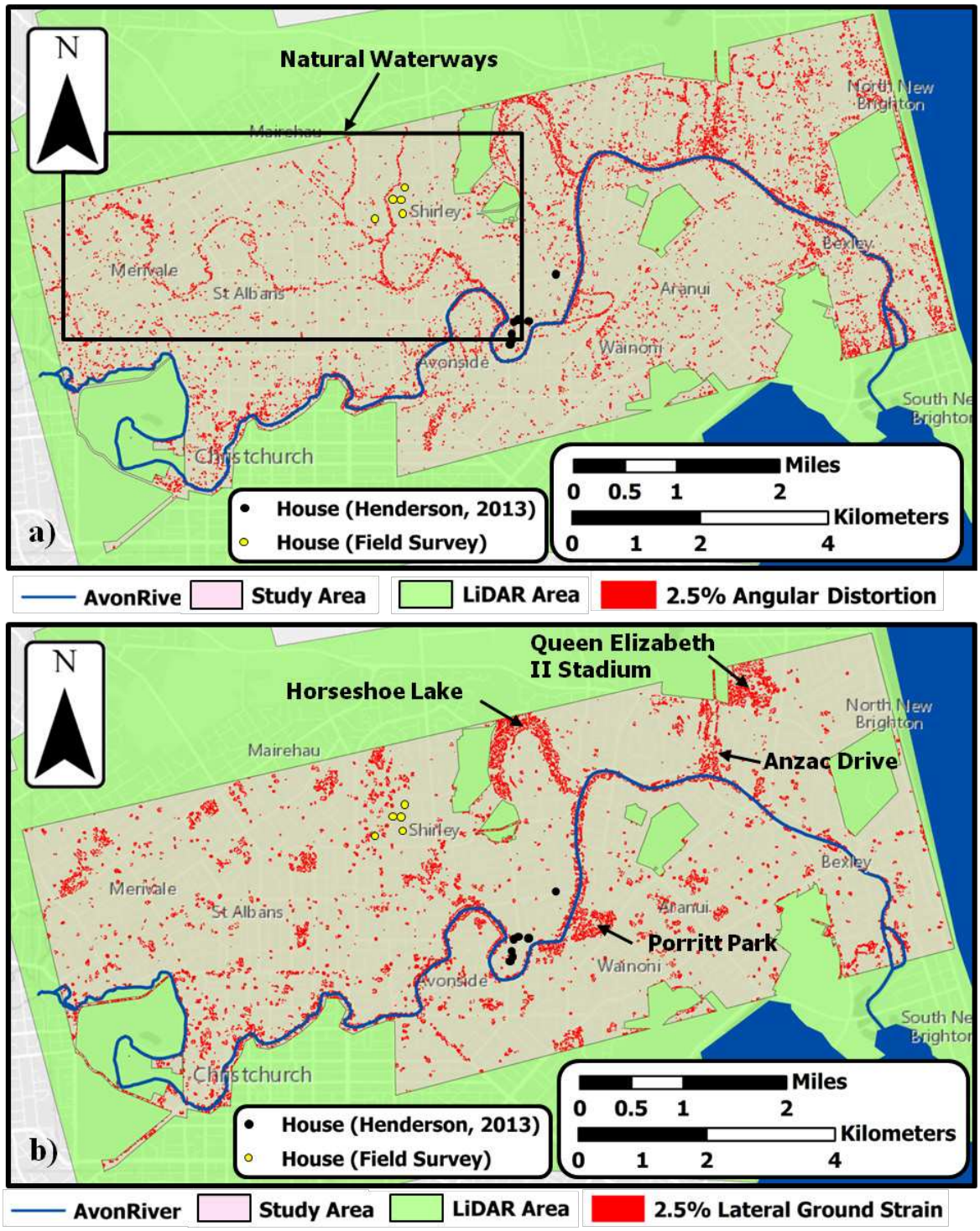


Figure 4: Spatial distribution of the 2.5% exceedance values of a) ground angular distortion, and b) lateral ground strain caused by the 22 Feb. 2011 earthquake in the study area.

Even small streams in Figure 4a, are delineated by the β locations. The 2.5% exceedance values of β provide a remarkably accurate measure for locating all sizes and types of natural water courses and previous meanders of the Avon River. In contrast, $\varepsilon_{HP}$ is not effective in locating streams. The $\varepsilon_{HP}$ data tend to cluster in small areas of vegetation.

## LiDAR-Based Ground Deformations vs Foundation Deformations

Five residential properties surveyed during June, 2013 in the Mairehau and Shirley neighborhoods of Christchurch are shown in Figures 4a and 4b in yellow. Seven houses, surveyed and described by Henderson (2013), are shown in Figures 4a and 4b in black.

During the June 2013 survey, vertical cracks > 2 mm in thickness along each concrete perimeter foundation wall were assumed to represent extension displacement, half of which was allocated to each end. Orthogonal movements in the x- and y- directions at each corner of the rectangular foundation were estimated from these displacements, and used in quadrilateral finite element formulations to calculate lateral strains in accordance with Figure 5. The absolute maximum value of principal lateral ground strain, $\varepsilon_{HPB}$, was used to represent foundation lateral strain in each building.

LiDAR measurements collected before the 4 Sept. 2010 and after the 23 Dec. 2011 earthquakes were used to assess $\varepsilon_{HP}$. The 4-m cells for $\varepsilon_{HP}$ estimates at each building were identified in ArcMap, and the average $\varepsilon_{HP}$ corresponding to each building footprint was calculated.

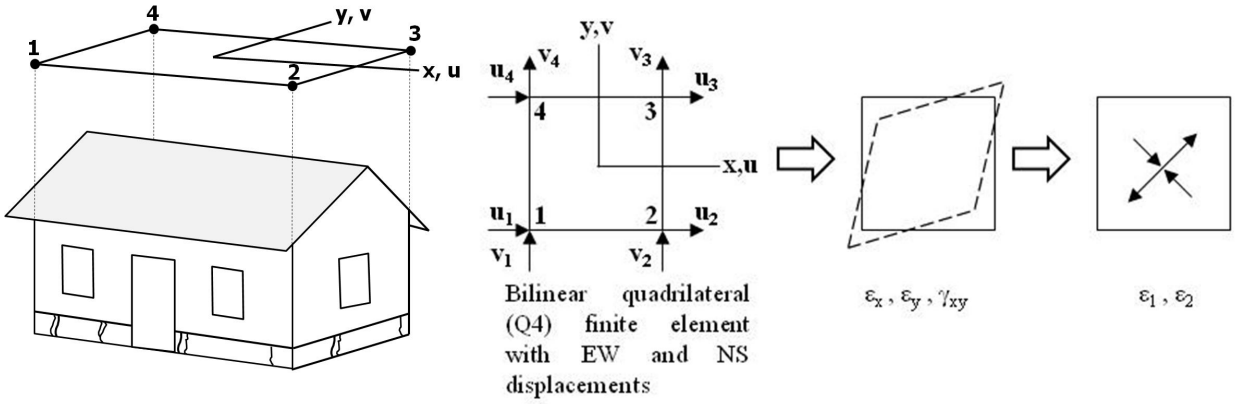


Figure 5: Calculation of lateral strains at surveyed residential buildings using quadrilateral finite element formulations.

Foundation differential vertical displacements were calculated with survey data for the ground floors. Contour of differential vertical displacement in 10-mm increments were developed in ArcMap. Figure 6 shows differential vertical displacement contours for a building with a slab on grade foundation. The contours are for two residences separated by a central garage. Equivalent floor slopes were calculated as shown in Figure 6. LiDAR measurements for the combined effects of the 4 Sept. 2010, 22 Feb. 2011 and 13 June 2011 earthquakes were used to estimate β and compared with the equivalent floor slopes.

Foundation lateral strain, $\varepsilon_{HPB}$, and the absolute value of maximum lateral ground strain, $\varepsilon_{HP}$, are plotted in Figure 7a for three buildings with concrete perimeter footings inspected in this study. Equivalent floor slope and angular distortion, β, are plotted for the 12 buildings under study in Figure 7b. Three of the five buildings surveyed in this study were divided into two living units with partitioning similar to that shown in Figure 6, and each part was considered as a separate data point in Figure 7b resulting in 15 data points in the figure.

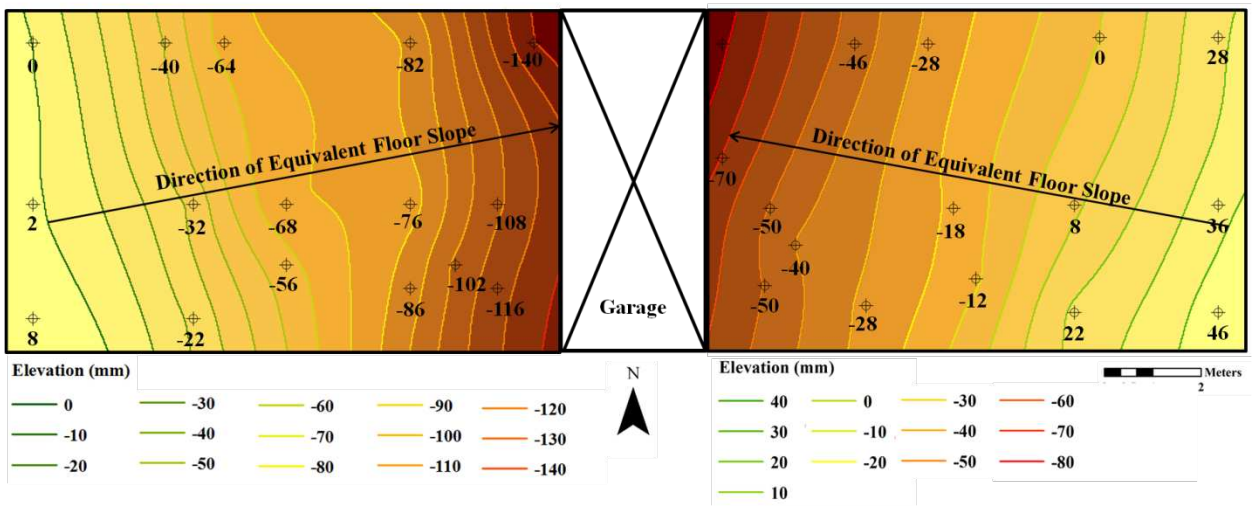


Figure 6: Contour plots of differential vertical displacement on the ground floor of a surveyed building with two individual residences and their equivalent floor slopes.

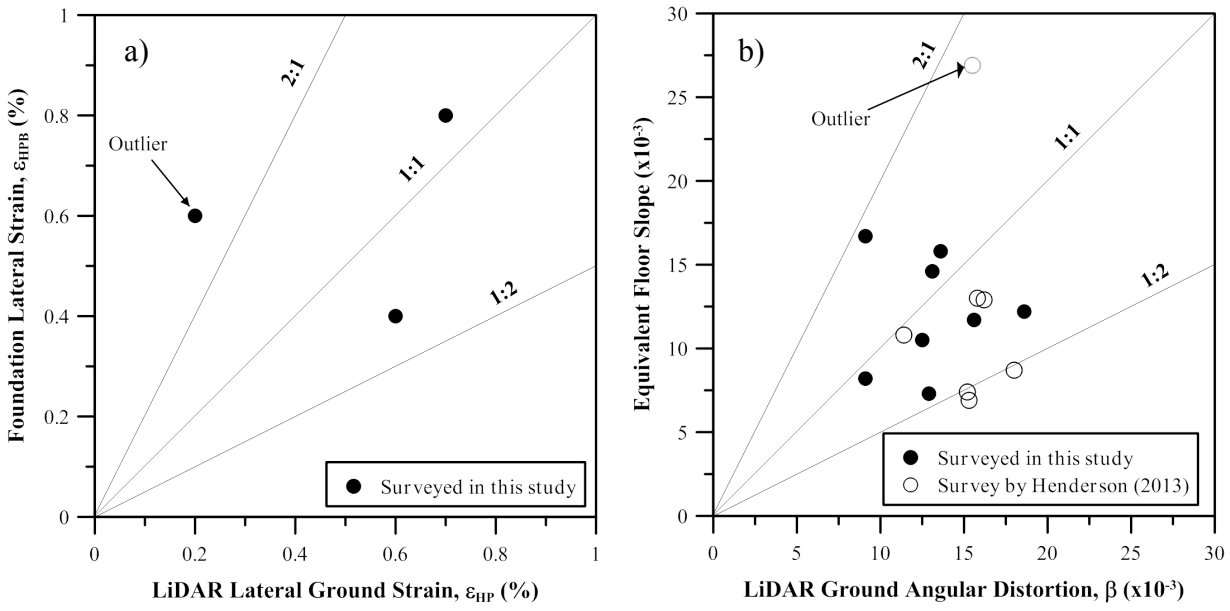


Figure 7: a) Foundation vs ground lateral strain, b) equivalent floor slope vs ground angular distortion.

The data summarized in Figure 7, although sparse, are in broad agreement overall. About 73% of the data are below the 1:1 line, which reflects the ability of a timber building to bridge over locally high settlements with floor slopes less than or equal to the ground angular distortion. In Figure 7a, the data point plotting above the 2:1 line represents a residence where cracking from lateral spreading increased the foundation lateral strain. The outlier in Figure 7b represents a house where concrete perimeter foundation corners were cracked and completely separated from the rest of the foundation. Localized foundation detachment and settlement in this case increased the equivalent floor slope well above the average distortion in the surrounding ground.

## Conclusions

The principal findings of this paper are:

- Statistical analysis of LiDAR ground movements indicates that liquefaction-induced ground deformation was locally most severe for the 4 Sept. 2010 earthquake, but aerially most extensive for the 22 Feb. 2011 earthquake.
- The generalized extreme value (GEV) distribution provides a good fit for $\beta$ and $\varepsilon_{HP}$ for the CES main earthquakes and may be used as an effective statistical distribution tool.
- Locations of highest $\beta$ are in remarkable agreement with those of existing water courses in Christchurch and provide a reliable means for locating all sizes and types of natural waterways and previous meanders of the Avon River.
- Liquefaction-induced $\beta$ and $\varepsilon_{HP}$ from LiDAR measurements show considerable scatter but are in broad agreement with concrete perimeter lateral strains and differential vertical ground floor displacements, respectively, interpreted from building damage surveys. Additional data will enhance the existing measurements and further exploration of the relationship between LiDAR and ground survey estimates of building deformation is recommended.

## Acknowledgments

The work described in this paper was supported by the National Science Foundation (NSF) under Award No. 1137977 and the U.S. Geological Survey (USGS) under Grant No. G12AP20034.

## References

Beavan J, Levick S, Lee J JK. *Ground displacements and dilatational strains caused by the 2010-2011 Canterbury earthquakes*. GNS Science Consultancy Report 2012/67, 2012: p. 59.

Bouziou D. *Earthquake-induced ground deformation effects on buried pipelines*. PhD Thesis. Cornell University: Ithaca, New York, 2015.

Boscardin MD, Cording EJ. Building response to excavation-induced settlement. Journal of Geotechnical Engineering 1989; **115**(1):1-21.

Canterbury Earthquake Recovery Authority (CERA). *Geotechnical database for Canterbury Earthquake Sequence*, NZ, available at: https://canterburygeotechnicaldatabase.projectorbit.com. [accessed June 2012]

Henderson DRK. *The Performance of House Foundations in the Canterbury Earthquakes*. M.Eng. Thesis. University of Canterbury: Christchurch, New Zealand, 2013.

Land Information New Zealand (LINZ). http://www.linz.govt.nz/. [accessed March 2013]

O'Rourke TD, Jeon S-S, Toprak S, Cubrinovski M, Hughes M, van Ballegooy M, Bouziou D. Earthquake Response of Underground Pipeline Networks in Christchurch, NZ. *Earthquake Spectra* 2014; **30**(1):183-204.